where the left lung does not wrap, and the septal-to-lateral wall count ratio is greater than one. This case probably results from the significantly larger path that the rays most important in defining the lateral wall must pass through. Our results, however, have been remarkably consistent. All 10 patients with left lung wrap-around (Fig. 5) have a hot lateral wall.

Three-dimensional studies with all sources of degradation modeled will further contribute to our understanding of SPECT imaging artifacts. In our study, a single mid-ventricular slice was used in order to isolate the lung wrap-around effect. The anatomical relationship between lung and heart depends on the slice position. By our observations of many PET transmission and emission images, less left lung wrap-around is seen for more inferior transaxial slices. Therefore, we might expect the hot lateral wall artifact in SPECT normal files to be more pronounced in the anterolateral region compared to the inferolateral region.

CONCLUSION

This use of transmission and emission PET ^{82}Rb data to create attenuated SPECT ^{201}Tl patient data demonstrates that the left lung wrapping around the lateral wall of the left ventricle correlated with the increased counts in the lateral wall seen in SPECT files for normal men and women.

REFERENCES

1. DePuey EG, Garcia EV. Optimal specificity of thallium-201 SPECT through recognition of imaging artifacts. *J Nucl Med* 1989;30:441–449.
2. Eisner RL, Tamas MY, Cloninger K, et al. The normal SPECT thallium-201 bullseye display: gender differences. *J Nucl Med* 1988;29:1901–1909.
3. Manglos SH, Thomas FD, Hellwig BJ. Phantom study of breast tissue attenuation in myocardial imaging. *J Nucl Med* 1993;34:992–996.
4. Nowak DJ. Attenuation cause and effect relationships in cardiac SPECT imaging. In: *1st International Congress of Nuclear Cardiology*. Cannes, France: 1981.
5. Nuyts J, Dupont P, Van den Maegdenbergh V, et al. A study of the liver-heart artifact in emission tomography. *J Nucl Med* 1995;36:133–139.
6. Tsui BMW, Zhao XD, Gregoriou GK, et al. Quantitative cardiac SPECT reconstruction with reduced image degradation due to patient anatomy. *IEEE Trans Nucl Sci* 1994;41:2838–2844.
7. Zhao XD, Tsui BMW, Gregoriou GK, et al. Evaluation of corrective reconstruction methods using a 3D cardiac-torso phantom and bulls-eye plots. *IEEE Conference Record of the 1993 Nuclear Science Symposium and Medical Imaging Conference*. 1993; 2:1164–1168.

Automatic Preparation of Radiopharmacokinetic Data for In Vivo Estimation of Receptor Biochemistry

Jing Chun Xu, David R. Vera and Robert C. Stadalnik

Department of Radiology, University of California, Davis Medical Center, Sacramento, California

We present a fully automated region of interest (ROI) and motion correction program for the generation of heart and liver time-activity data resulting from a hepatic functional imaging study using [^{99m}Tc-]galactosyl-neoglycoalbumin (^{99m}Tc-NGA). **Methods:** The program automatically draws heart and liver ROI and corrects for lateral movement of the subject. Eighty-four ^{99m}Tc-NGA studies, consisting of 32 healthy subjects and 52 patients with liver disease, were processed and submitted to an automated kinetic analysis that estimates the subject's asialoglycoprotein receptor concentration $[R]_o$. **Results:** When compared to time-activity data generated by operator-drawn ROIs without motion correction, the average reduced Chi-square of the kinetic analysis decreased significantly ($p < 0.001$) from 2.20 to 1.37 and the number of studies that satisfied quality control increased from 74 to 81 studies. Receiver operating characteristic of $[R]_o$ resulted in greater detectability (0.984 ± 0.012 compared with 0.965 ± 0.020) when automatic ROI generation was employed. Using the test criteria of 0.65 μM, the sensitivity of $[R]_o$ increased from 0.88 to 0.92 and the specificity increased from 0.96 to 0.97. **Conclusion:** Automated definition of liver and heart ROIs with motion correction, that reduces observational noise, increased the success rate of the radiopharmacokinetic analysis from 88% to 96%.

Key Words: technetium-99m-NGA; kinetic modeling; automatic motion correction; automatic contour detection

J Nucl Med 1996; 37:1896–1902

Technetium-99m-galactosyl-neoglycoalbumin (^{99m}Tc-NGA) is a receptor-binding radiopharmaceutical (*1*) specific for the asialoglycoprotein receptor (ASGP-R) (*2*) that resides exclusively at the cellular membrane of hepatocytes. Consequently, a healthy liver will accumulate an excess of 90% of the dose within 15 min, whereas a diseased liver will accumulate significantly less activity during the same time period (*3*). In addition to high cellular specificity (*4*), another unique feature of ASGP-R is a lack of pharmacologic response to ligand binding. This feature enabled us to inject ^{99m}Tc-NGA in amounts that would occupy a significant fraction of ASGP-R. Consequently, we are able to operate the radiopharmacokinetic system as a bimolecular reaction (*5*), which permits high-precision measurements (*6*) of receptor concentration (*7,8*) from liver and heart time-activity data (*9*). Clinical studies have demonstrated that receptor concentration can differentiate (*10–13*) between healthy subjects and patients with liver disease. The largest study (*14*) reported to date, comprising 32 healthy volunteers and 52 patients, yielded a sensitivity of 88% for the detection of noncholestatic liver disease. The specificity was 96%.

Routine widespread clinical application of ^{99m}Tc-NGA pharmacokinetic modeling will require a fully automated analysis. One component of an automated analysis is the preparation of liver and heart time-activity curves, that provide the primary data for the pharmacokinetic analysis. This process requires two steps: (a) define the liver and heart regions of interest (ROIs) and (b) generate the time-activity curves by summing the counts within each ROI at every frame within the dynamic imaging study. Previous ^{99m}Tc-NGA functional imaging studies used standard nuclear medicine software with which the liver and heart ROIs were manually defined by lightpen and the time-activity curves were generated without correction for patient motion. Automation of this process would have two significant

Received May 26, 1995; revision accepted Jan. 28, 1996.

For correspondence or reprints contact: Robert C. Stadalnik, MD, Division of Nuclear Medicine, Research I Building, Rm. 1001, 4635 Second Ave., University of California, Davis, Medical Center, Sacramento, CA 95817.

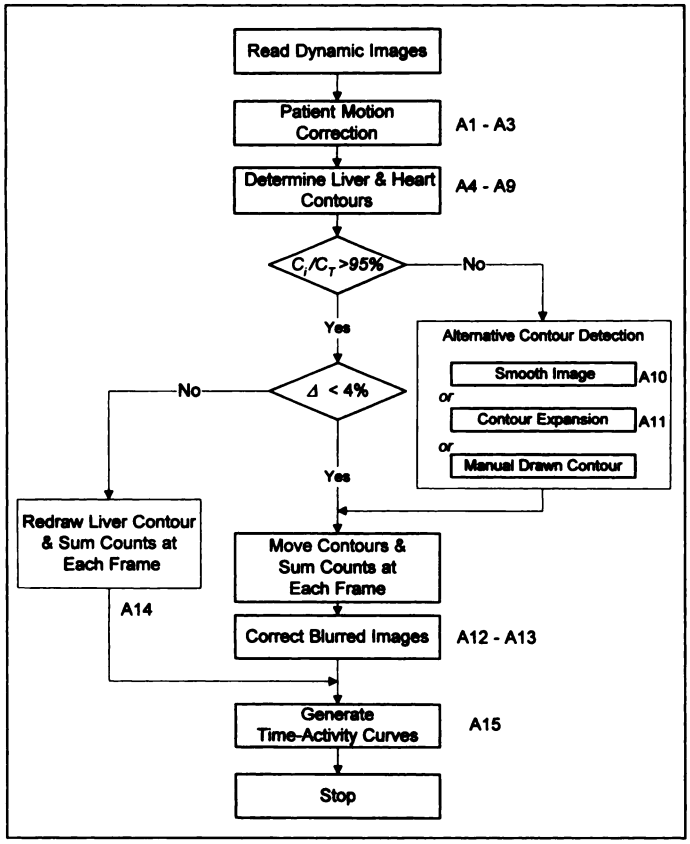

FIGURE 1. Algorithm for program PRDIVA that automatically prepares a ^{99m}Tc-NGA dynamic imaging study for estimation of receptor concentration. Primary path is the vertical set of boxes. Pertinent equations (Appendix) are indicated at each step.

benefits. First, automatic definition of the liver and heart ROIs would eliminate operator bias. Second, an automated program would permit the correction of each ROI for patient movement during the 30-min imaging study. There are three types of lateral patient movement that could be corrected by an automated process. The first, and most common, are small motions of a constant rocking nature. If an ROI using a fixed position is used, this motion increases the noise of the time-activity data. The second type of movement is a sudden, large but momentary change in position; this causes a spike in the time-activity curve. These first two types of motion are potential sources of measurement bias, decrease measurement precision, and degrade the quality of the resulting kinetic analysis. As a result, if the noise is abnormally high and multiple spikes are present in the time-activity data, the resulting kinetic analysis may not pass the criteria we set to ensure the technical quality of the kinetic analysis (*14*). The third type occurs when the patient moves and does not return to the original position; this causes an abrupt offset in the time-activity curves. This type of patient movement yields time-activity data that can not be successfully analyzed for receptor concentration by the radiopharmacokinetic model.

We present and test an algorithm that automatically defines the heart and liver ROIs from a ^{99m}Tc-NGA functional imaging study and adjusts the ROIs at each frame. Our primary goal was to eliminate of operator bias and reduction in the number of studies that fail the receptor concentration analysis due to patient movement. The overall result was a decrease in the noise of the time-activity data and a higher success rate for the radiopharmacokinetic analysis.

TABLE 1
Symbols

Symbol	Designation	Units*
A	ROI area	l^2
A_b^k	Blurred area	l^2
Ave1 (x_i,y_j),	Summed image	cts
Ave2 (x_i,y_j),	Summed image	cts
$\mathbf{I}_{liv}(x_i, y_j)$	Masked image	cts
$\mathbf{I}_{hrt}(x_i, y_j)$	Masked image	cts
k	Frame number	
L_c	Contour threshold	cts
$\mathbf{M}(x_i, y_j)$	Image mask	
R_{liv}^k	Contour (liver)	l
R_{hrt}^k	Contour (heart)	l
W_{cb}^k	Blurring correction	
W_{liv}^k	Total counts within liver contour	cts
W_{hrt}^k	Total counts within heart contour	cts
$\hat{W}_{liv}^k, \hat{W}_{hrt}^k$	Prediction calculated for model	cts
x_i, y_j	x, y position	l
X_c^k, Y_c^k	x, y component of center of mass in kth frame R_c^k	l
X_0^k, Y_0^k	x, y component of the patient's motion in kth frame R_0^k	l
Δt	Frame duration	min
Δx	Distance	l
$\sigma^k(x_i, y_j)$	Counts at x, y position in kth frame	l

*l = length.

MATERIALS AND METHODS

Algorithm

Designated as PRDIVA (preparation of radiopharmacokinetic data in vivo automatically), the image processing program automatically defines the liver and heart ROIs and then automatically corrects each ROI for patient motion during the dynamic imaging study. The algorithm consists of several steps which are illustrated in Figure 1. First, PRDIVA reads the dynamic images, and then calculates the misalignment of each frame of image due to the patient's lateral motion. In the next step, PRDIVA determines the liver and heart contours. If a contour encloses less than 95% of the total counts above a predefined threshold ($C_i/C_T < 95\%$), the contour is considered ill-defined and PRDIVA automatically selects one of two alternative methods for determining the liver and heart contours. The first alternative is the application of a spatial filter to smooth the image. The second alternative is the application of a nonlinear transformation that gradually expands the contour. If the criterion C_i/C_T can be met using either alternative, PRDIVA continues to process images; otherwise, PRDIVA requests that heart and liver contours be defined manually. If the contours are well-defined without using either alternative, PRDIVA compares the liver displacement during the study to determine if the contours should be redrawn at each frame, or if the contours can be repositioned at each frame. The latter method is significantly faster. The criterion is a unitless ratio, $\Delta = \Delta x/\sqrt{A}$ where A is the mean of the area within the liver contour obtained at the beginning and end of the study and Δx is the distance between the two geometric centers. If the ratio is larger than 4%, PRDIVA redraws the liver contour at each frame. Otherwise, PRDIVA moves the contours to follow the patient's motion and corrects blurred images. Finally, PRDIVA generates a time-activity curve for each ROI. A complete mathematical description of the algorithm is given in the Appendix. The symbols used in this paper are listed in Table 1.

Implementation

PRDIVA was implemented in IDL (Research System Inc., Boulder, CO) and was tested in DEC 3000 AXP (Alpha 200 MHz, Digital Equipment Company, Danvers, MA) running OpenVMS, and PC486DX (50 MHz). When the moving contour was applied, PRDIVA required less than 20 sec when running on a DEC 3000 and 1 min on the PC. When the redraw contour alternative was used, the program required 2 and 10 min on the DEC 3000 and PC, respectively.

Experimental Design

PRDIVA was tested in the following manner. Unmodified dynamic images resulting from 84 ^{99m}Tc-NGA functional imaging studies (*1*) were submitted to PRDIVA for generation of heart and liver time-activity curves. The resulting curves were then submitted to the program NGAFIT (*9*), which automatically performed a nonlinear regression of the ^{99m}Tc-NGA kinetic model to the heart and liver time-activity data. The subjects studied were the same as in a previous report (*14*) that used operator-defined ROIs. Of the 84 subjects, 32 were healthy individuals and 52 had varying degrees of histologically-proven cirrhosis or hepatitis. Only one ^{99m}Tc-NGA study from each subject was included in the 84 studies. The curve fit results were accepted only if the following conditions were met: (a) the total reduced chi square (weighting based on Poisson distribution) was less than 2.85; (b) $[R]_o$ was less than 0.5 μM, the chi square criterion was set to 3.25, or if $[R]_o$ was less than 0.4 μM, the criterion is set to 3.5. All studies used at least one blood sample drawn between 3 and 5 min after injection.

Statistical Analysis

Two methods were used as performance measures of the automated ROI program. In the first method, the total reduced chi square [Equations 8 and 10 from Vera et al. (*15*)] resulting from curve fits to time-activity data from the automated program were compared to the operator-drawn ROIs by the paired Student's t-test.

As a second method, we used receiver operating characteristic (ROC) analysis (*16*) to compare the diagnostic performance of the receptor concentration $[R]_o$ estimates obtained from curve fits to PRDIVA-generated time-activity data and $[R]_o$ estimates from time-activity curves from manually drawn ROIs. Program CLABROC was used to generate a set of ROC operating points for $[R]_o$ from each method, to perform a binormal fit to each set of operating points and to calculate the area A_z under each binormal curve. The statistical significance of the difference in diagnostic performance was tested using CLABROC. The CLABROC algorithm, developed by Metz, is a version of the CORROC algorithm (*17*) that has been modified to analyze continuously distributed data (*18*). In addition, we tested the precision of the estimated difference in A_Z by calculating a 95% confidence interval (*19*). Calculations of p and the confidence interval were conducted with an input dataset that did not include $[R]_o$ values from the seven ^{99m}Tc-NGA studies that passed kinetic analysis quality control after PRDIVA processing but failed quality control using time-activity curves for manually-drawn contours. The elimination of these studies from the statistical analysis assumed that these studies were not atypically difficult or easy cases (Metz CE, *personal communication).*

RESULTS

Algorithm

The algorithm, as illustrated in Figure 1, uses two methods to correct for patient motion. We will describe the processing of a ^{99m}Tc-NGA study from a healthy subject and a patient suffering from hepatitis to illustrate the different methods. In the healthy subjects, the liver completely extracts the radiopharmaceutical.

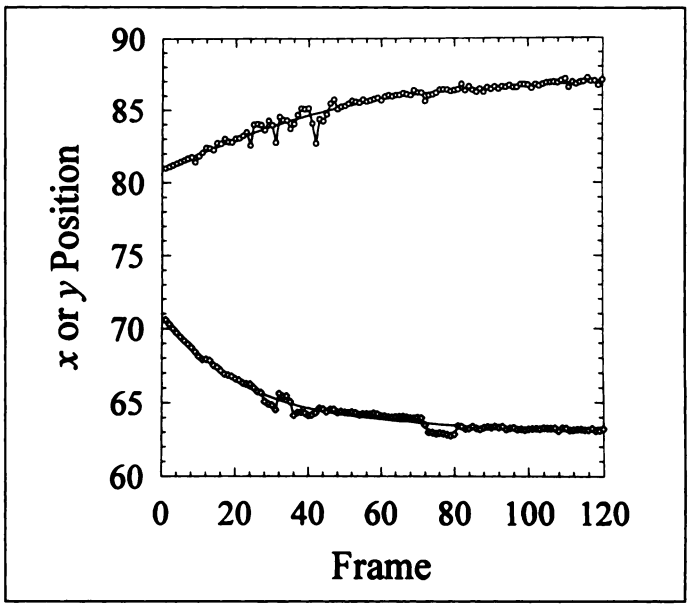

FIGURE 2. The x and y components of the image center were determined by a third-order least square fit (smooth curves) to the liver time-activity curve (◇ = x, ○ = y). There are movements around Frames 40 and 80.

As a result, the liver will be the only structure to appear in the last 15 min of the 30-min study. In this study, the program redraws the liver contour at each frame. In patients with liver disease, both the liver and blood pool structures appear in the final frame. Under this condition, the program corrects for motion by repositioning the heart and liver contours for each frame.

Healthy Subject. The motion correction for a healthy subject, shown as Figure 2, indicates movement around Frames 40 and 80. Figure 3 contains images pertinent to the processing of this subject: A is the image at the beginning of the study, B at the end of study, C the heart image ($\mathbf{I}_{hrt}$ described in Eq. A9); D the liver image ($\mathbf{I}_{liv}$ described in Eq. A5). Since the liver contour was well-defined at D ($C_i/C_T < 95\%$), there was no need to use any of the alternative methods to determine the liver contour. Therefore, PRDIVA continued with the algorithm and tested the displacement criteria (Eq. A5), which determines if repositioning of the contours at each frame will be sufficient. Because the

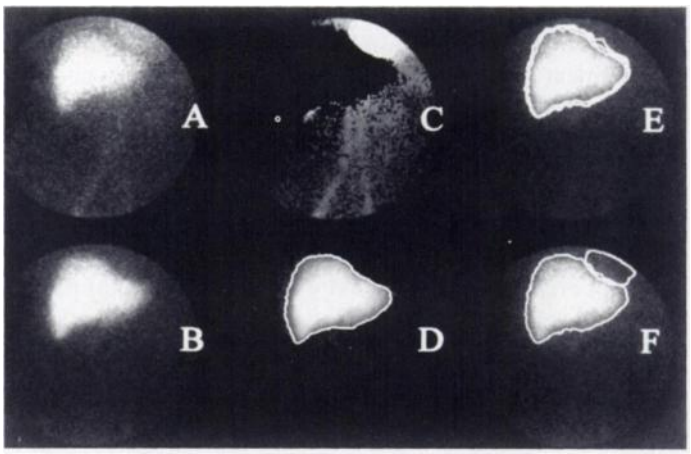

FIGURE 3. Program PRDIVA automatically draws contours for the liver and heart. Images at the (A) beginning and (B) end of the study are shown. Masked images $\mathbf{I}_{hrt}$ and $\mathbf{I}_{liv}$ are used by PRDIVA to define the (C) heart and (D) liver contours. Because of the large lateral motion at Frame 42 (Fig. 2), PRDIVA redrew the liver contour for each frame. The three contours in E with different L_c illustrated how PRDIVA redrew the contour at the last frame. The final contours of this frame are illustrated in F.

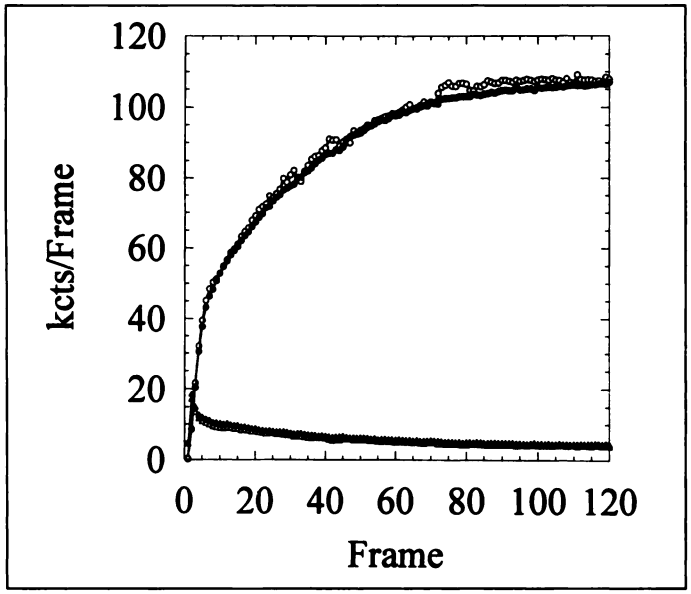

FIGURE 4. Automated liver and heart contour detection at each frame of the dynamic study by PRDIVA resulted in smoother time-activity curves (closed symbols) than the curves that are generated by manually-defined (open symbols) liver (circles) and heart (triangles) ROIs. The curve fit to the manually defined ROI data did not pass quality control criteria due to an excessively high reduced chi square; the PRDIVA-generated ROI data yielded a curve fit that passed quality control.

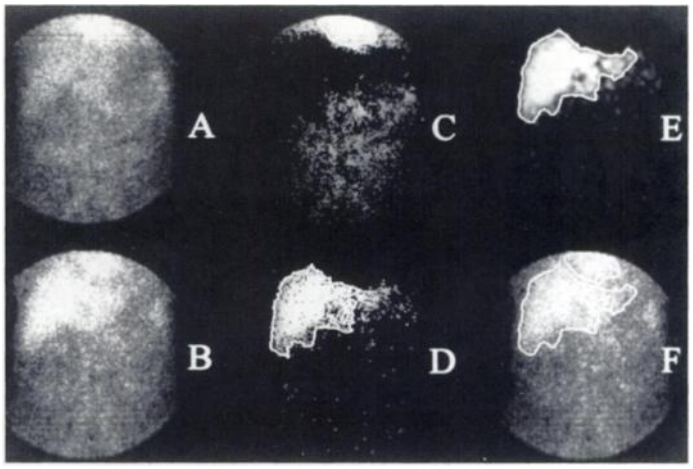

FIGURE 5. Because the liver contour did not enclose at least 95% of the counts in the masked image, PRDIVA smoothed I_{liv} to produce the masked image at E and a new liver contour. The program then corrected for the patient's motion by adjusting the position of each contour to the center of mass of each frame. F is the last frame of the Tc-NGA study with the heart and liver contours.

displacement of the liver contour, $\Delta = \Delta x/\sqrt{A}$, was larger than 4%, PRDIVA redrew the liver contour for each frame. This procedure is illustrated in Figure 3E with three liver contours corresponding to L_c values of 13, 15 and 22. PRDIVA automatically adjusted L_c to 15, which produced an area that was larger than 94% and less than 106% of liver contour area defined in Figure 3D. The liver and heart contours are illustrated in Figure 3F. This condition was satisfied at each frame. The time-activity curves generated by PRDIVA are shown in Figure 4. Using manually-defined ROIs, this study was previously rejected due to a poor fit ($\chi^2_\nu = 8.79$). The PRDIVA-generated time-activity curves resulted in an acceptable reduced chi square ($\chi^2_\nu = 1.86$) and yielded a normal receptor concentration ($[R]_o = 0.879\ \mu M$) after parameter estimation by program NGAFIT.

Patient with Hepatitis. The images of a patient suffering from hepatitis are illustrated in Figure 5, where A is at the beginning of the study, B is the last frame, and C and D are heart $\mathbf{I}_{hrt}$ (Eq. A9) and liver images $\mathbf{I}_{liv}$ (Eq. A5), respectively. Using edge detection, as previously described, PRDIVA drew the (C) heart contour from image $\mathbf{I}_{hrt}$ and the (D) liver contour from $\mathbf{I}_{liv}$. Because the liver contour did not enclose 95% of the total points above the predefined threshold ($C_i/C_T < 95\%$), PRDIVA considered the contour as ill-defined and smoothed this image (D) as illustrated in Figure 5E. Using this smoothed image, PRDIVA was able to define the liver contour to satisfy the threshold criteria. The defined liver and heart contours are shown in Figure 5F. Having satisfied the threshold criteria, PRDIVA continued to reposition liver and heart contours at each frame. The results of NGAFIT indicated a decrease in χ^2_ν from 1.85 to 1.33 using data generated by PRDIVA.

Experimental Design

Ninety-six percent of the ^{99m}Tc-NGA studies processed by PRDIVA passed the curve-fit criteria. This was the same criteria used in the previous report that used manually-defined heart and liver contours from the same set of ^{99m}Tc-NGA studies. The success rate of the time-activity curves from manually-defined ROIs was 88%. In 7 of the 84 ^{99m}Tc-NGA studies, PRDIVA requested operator intervention for manual definition of heart and liver contours; all of these studies were of patients with severe liver disease. Twenty-one studies employed the redraw contour mode, which redefines the liver contour at each frame, and therefore required a longer execution time. Seventy-six percent of the studies resulted in better curve fits with PRDIVA-generated curves.

The automated program altered the clinical diagnosis. Of the ^{99m}Tc-NGA studies that passed the kinetic analysis quality criteria using the manual method, one false-positive study became a true negative and four false negatives became true positives. The seven ^{99m}Tc-NGA studies that passed the kinetic analysis quality criteria only after PRDIVA analysis had the following outcomes: two true negatives, one false positive, two true positives and two false negatives. The diagnoses were based on a $[R]_o$ decision criteria of 0.65 μM.

Statistical Analysis

The average χ^2_ν decreased by 38% from 2.20 to 1.37. Based on the paired Student's t-test, χ^2_ν resulting from PRDIVA-generated time-activity curves was significantly ($p < 0.001$) lower than the reduced chi square of curves from manually-defined ROIs. Automatically defined ROIs yielded a wider separation (Fig. 6A) between $[R]_o$ measurements of healthy subjects and patients when compared to $[R]_o$ measurements from manually drawn ROIs. The mean $[R]_o$ for healthy subjects using PRDIVA was $0.811 \pm 0.107\ \mu M$; using manually-drawn ROIs, the mean $[R]_o$ was $0.826 \pm 0.121\ \mu M$. The mean $[R]_o$ for patients using PRDIVA was $0.424 \pm 0.127\ \mu M$; using manually-drawn ROIs, the mean $[R]_o$ was $0.438 \pm 0.152\ \mu M$. When PRDIVA was used to generate the time-activity data, the coefficients of variation decreased for healthy subjects (0.13 versus 0.15) and patients (0.30 versus 0.35).

By using a test criteria of 0.65 μM, the sensitivity of $[R]_o$ increased from 88% to 92% and the specificity increased from 96% to 97%. Accuracy increased from 0.92 to 0.94. Receiver operating characteristic analysis of $[R]_o$ (Fig. 6B) indicated higher diagnostic performance with PRDIVA-generated time-activity data. The area under the ROC curve produced by receptor concentrations estimated from PRDIVA-generated time-activity data was 0.984 ± 0.012; the area under the ROC

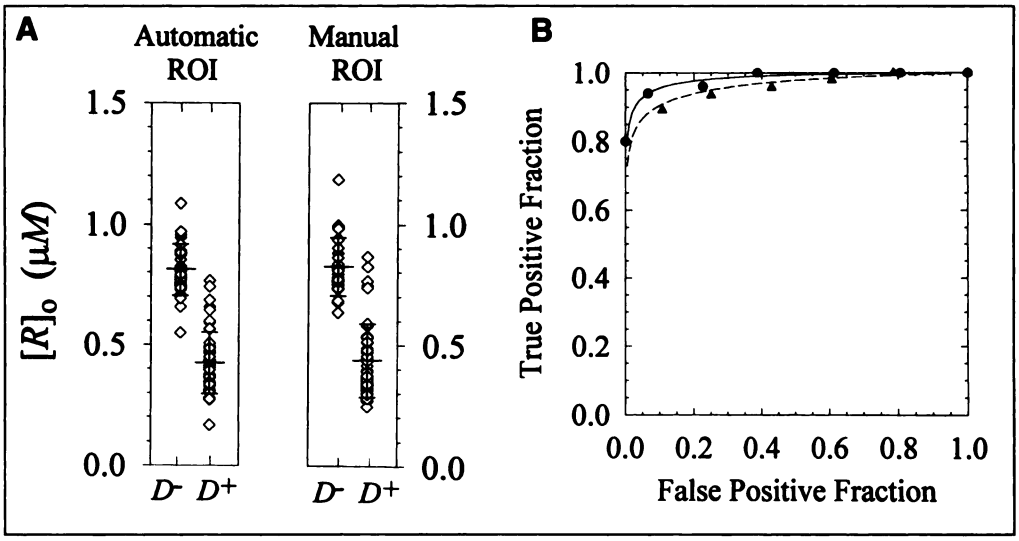

FIGURE 6. Automatically defined ROIs yielded a wider separation between $[R]_o$ measurements of healthy subjects and patients when compared to $[R]_o$ measurements from (A) manually drawn ROIs. (B) Receiver operating characteristic (ROC) analysis demonstrated higher detectability of $[R]_o$ when the liver and heart time-activity curves were generated via automatic edge detection and correction for patient motion. The circles represent the ROC operating points for the automated process, and the smooth line is a binormal fit. The triangles represent the ROC operating points for $[R]_o$ when the time-activity data are defined manually and there is no correction for patient motion. The dashed line is the binormal fit to the ROC curve.

curve produced by $[R]_o$ from manually drawn ROIs was 0.959 ± 0.022.

The ROC analysis was not able to prove superior diagnostic accuracy from either method, nor could they be proved equivalent. Using a completely paired dataset, the PRDIVA-based $[R]_o$ values yielded a ROC curve with an A_Z of 0.997 ± 0.004. The two-tailed p level was 0.081. Based on a typical $P_{critical}$ of 0.05, a p of 0.081 is cause to accept a null hypothesis of no difference in diagnostic performance. The confidence interval, which is used to establish that two methods are equivalent (*20*) was inconclusive. The 95% confidence interval was [−0.005, 0.084]. Based on a maximum confidence interval of [−0.075, 0.075], we must conclude that the sample size was not adequate to demonstrate a lack of clinical significance.

DISCUSSION

Our approach to motion correction and detection is different from the three-dimensional surface fitting developed by Scott et al. (*21*) for image registration of SPECT and CT images. This method can produce accurate alignment by applying an algorithm developed by Pelizzari et al. (*22*) that allows for translation, rotation and scaling in the x-y plane, as well as for movement in the *z* axis. Our motion correction program does not correct for patient rotation or movement along the *z* axis, since we do not believe they are a problem in data acquisition.

Starting from the maximum points inside the object, our contour program is different from the edge detection algorithm for MR images developed by Turkington et al. (*23*), where a manually drawn rough polygon around the object is required. They apply edge detection to one image frame, while we generate a one-object image; that is, the difference between an early image and a late image (Fig. 3C, D; Fig. 5C, D). Since the background level is significantly reduced, the criterion of a well-defined contour is whether it can enclose all the points above a certain threshold, i.e. C_i/C_o. For an ill-defined contour, PRDIVA automatically applies two alternative methods, smoothing and expansion. The limitation for automated contour determination is set to four neighbors in expansion. Beyond this point, we believe that the automatically-drawn contour is not reliable and manual drawing of contours is required. We did not test our contour algorithm for boundary accuracy. There are two reasons why the accuracy of the organ boundary is not critical for the measurement of receptor concentration. First, because the magnitude of $[R]_o$ is encoded into the shape of the liver and heart time-activity data, it is insensitive to the size of the ROI or the ability of the ROI to exactly describe the liver boundary. Second, $[R]_o$ represents an average value of receptor concentration throughout the entire liver. Consequently, we attempt to sample the entire liver. However, if a small portion of the organ is not included within the contour, the probability is extremely low that its receptor concentration will significantly alter the shape of the time-activity curve.

Statistical analysis of the ROC curves requires two comments. First, the analysis used completely paired data and therefore did not include the seven studies that failed the kinetic analysis when the liver and heart time-activity data were generated by manually-drawn ROIs. This was carried out because CLABROC cannot provide a statistical analysis of datasets in which some of the entries are not paired. Consequently, the statistical calculations are valid only if the seven studies deleted from the analysis were not atypically easy or difficult. The fact that these studies could not pass the kinetic analysis quality criteria without automated correction for patient movement does not argue against this assumption. In other words, the fact that a subject decided to move slightly during the ^{99m}Tc-NGA study is not indicative of an easy or a difficult case. We assume that, if the assumption is not appropriate, an increase in p value and the 95% confidence interval would result.

The second point regarding the ROC analysis concerns the significance of the confidence interval analysis. Because our sole purpose for using PRDIVA was to increase the success rate of the kinetic analysis, a demonstration of equivalence in diagnostic performance will suffice. The lower bound (LB) of the 95% confidence interval provides an estimate of the possible decrease in performance using PRDIVA. Based on the current sample size, PRDIVA offers an 8% increase in the success rate of the radiopharmacokinetic analysis over manually prepared kinetic data. This increase in the success rate comes with a low probability (5%) that the diagnostic performance is decreased by 8% (ΔA_z/LB).

CONCLUSION

We have demonstrated that an algorithm of automatic ROI and motion correction for the generation of heart and liver time-activity data can reduce systematic error and thereby increase the success rate of the pharmacokinetic modeling process to 96%.

APPENDIX

Algorithm PRDIVA

We present a mathematical description of algorithm PRDIVA. Figure 1 is a flow chart with pertinent equations adjacent to each step. Table 1 contains a list of symbols with designations and units.

Motion Correction. Lateral motion during the imaging study is corrected by the following algorithm. The center of mass R_c^k for each frame is calculated as:

$$R_c^k = \frac{\sum_{i=1}^{n}\sum_{j=1}^{n} \sigma^k(x_i, y_j) r(x_i, y_j)}{\sum_{i=1}^{n}\sum_{j=1}^{n} \sigma^k(x_i, y_j)}, \quad \text{Eq. A1a}$$

where n is the image size, $\sigma^k(x_i, y_j)$ represents the counts collected at position r with coordinating x_i, y_i, and k is the frame number. The vector R_c^k can be separated to X_c^k and Y_c^k in Cartesian coordinates as:

$$X_c^k = \frac{\sum_{i=1}^{n}\sum_{j=1}^{n} \sigma^k(x_i, y_j)\, x_i}{\sum_{i=1}^{n}\sum_{j=1}^{n} \sigma^k(x_i, y_j)} \quad \text{Eq. A1b}$$

$$Y_c^k = \frac{\sum_{i=1}^{n}\sum_{j=1}^{n} \sigma^k(x_i, y_j)\, y_j}{\sum_{i=1}^{n}\sum_{j=1}^{n} \sigma^k(x_i, y_j)} \quad \text{Eq. A1c}$$

The x and y components of the center of mass (X_c, Y_c) are fitted to third order polynomials f_x and f_y,:

$$f_x = a_0 + a_1 * k + a_2 * k^2 + a_3 * k^3 \quad \text{Eq. A2a}$$

$$f_y = b_0 + b_1 * k + b_2 * k^2 + b_3 * k^3 \quad \text{Eq. A2b}$$

while residual a_0 through a_3 and b_0 through b_3 are calculated from general least square fit (*24*). The residual for each frame R_c^k corresponds to the patient's movement:

$$R_o^k = (X_o^k, Y_o^k = R_c^k(X_c^k, Y_c^k) - f(f_x, f_y) \quad \text{Eq. A3a}$$

$$X_0^k = X_c^k - f_x(k) \quad \text{Eq. A3b}$$

$$Y_0^k = Y_c^k - f_y(k) \quad \text{Eq. A3c}$$

Determination of Liver and Heart Contours. PRDIVA generates two images to define the liver and heart contour. Averaging Frames 3–5 as **Ave1** and Frames 117–110 as **Ave2**, mask $\mathbf{M}_1$ is defined as:

$$\mathbf{Ave2}(x_i, y_j) - \mathbf{Ave1}(x_i, y_j) > v_0, \quad \text{Eq. A4a}$$

$$\mathbf{M}_1(x_i, y_j) = 1 \quad \text{Eq. A4b}$$

$$\mathbf{M}_1(x_i, y_j) = 0, \quad \text{Eq. A4c}$$

where v_0 is the threshold set equal to background. The image used to draw liver contour $\mathbf{I}_{liv}$ is thus generated as:

$$\mathbf{I}_{liv}(x_i, y_j) = \mathbf{Ave2}(x_i, y_j) * \mathbf{M}_1(x_i, y_j). \quad \text{Eq. A5}$$

The threshold is set as:

$$L_c = 0.1s, \quad \text{Eq. A6}$$

where s is the average intensity around the maximum point of the image. From this maximum point, PRDIVA searches for the first point where the intensity falls below L_c along × direction ($\theta = 0$). Thus, the contour point r is expressed in polar coordinates as:

$$r = \rho\theta, \quad \text{Eq. A7a}$$

where ρ is the radius and θ is the polar angle. Starting from:

$$r = \rho(\theta + \delta\theta) \quad \text{Eq. A7b}$$

$$d\theta = 2\pi/300. \quad \text{Eq. A7c}$$

PRDIVA searches for the next contour point along $\theta+\delta\theta$ direction where the intensity changes from above to below L_c. Repeating this procedure 300 times to a full circle, PRDIVA encloses the contour $\mathbf{R}_{liv}$ around the maximum point. Array $\mathbf{R}_{liv}$ is a 2 × 300-dimensional array that holds the x and y components of each r. A second mask is generated to produce a heart contour image $\mathbf{I}_{hrt}(x_i, y_j)$:
if

$$\mathbf{Ave1}(x_i, y_j) - \mathbf{Ave2}(x_i, y_j) > v_0, \quad \text{Eq. A8a}$$

then

$$\mathbf{M}_2(x_i, y_j) = 1 \quad \text{Eq. A8b}$$

otherwise

$$\mathbf{M}_2(x_i, y_j) = 0. \quad \text{Eq. A8c}$$

Multiplying **Ave1** by $\mathbf{M}_2$, PRDIVA generates a heart image as follows:

$$\mathbf{I}_{hrt}(x_i, y_j) = \mathbf{Ave1}(x_i, y_j) * \mathbf{M}_2(x_i, y_j). \quad \text{Eq. A9}$$

From this image, PRDIVA defines the heart contour, R_{hrt}, using Equations A6 through A7.

At this point in the algorithm, PRDIVA calculates a metric that is used to determine if the contours properly circumscribe the liver and heart. If the liver contour encloses less than 95% of the total counts above the threshold L_c, PRDIVA implements one of two alternative methods to automatically determine the liver contour. First, PRDIVA smooths the liver contour image $\mathbf{I}_{liv}(x_i, y_j)$ with a two-dimensional 10 × 10 filter. Using the smoothed image, PRDIVA redraws the contour and checks the ratio C_i/C_T. If this ratio is greater than 95%, PRDIVA continues with the algorithm by applying a correction for patient motion. Second, if the ratio C_i/C_T is still <0.95%, a nonlinear transformation is then applied to $\mathbf{I}_{liv}(x_i, y_j)$:
if

$$\mathbf{I}_{liv}(x_i, y_j) > v_0, \quad \text{Eq. A10a}$$

then

$$\mathbf{I}_{liv}(x_i, y_j) = 100 \quad \text{Eq. A10b}$$

otherwise

$$\mathbf{I}_{liv}(x_i, y_j) = 0. \quad \text{Eq. A10c}$$

Then every nonzero point gradually expands up to its four neighbors to see if the following condition can be met:

$$C_o/C_i < 10\%, \quad \text{Eq. A11}$$

where C_o represents the nonzero points outside the contour and C_i represents the points inside. If this condition is met, PRDIVA continues with the algorithm; otherwise, the program requires that the operator manually draw the liver and heart contours. Manual definition of the liver and heart ROIs uses irregular contours that

circumscribe the liver or heart as viewed from the 40th frame (10-min PI) of the dynamic study.

Blurring Correction. The program corrects for blurring caused by patient movement of long duration. The blur correction W_{cb}^k, a unitless number, is defined as:

$$W_{cb}^k = V * (A_b^k - A)/A, \qquad \text{Eq. A12}$$

where A is the area of the ROI, A_b^k is the blurred area common to the kth and (k-1)th frames, and V, which ranged from 0 to 1, is defined as the velocity of:

$$V \propto \sqrt{(X_0^k - X_0^{k-1})^2 + (Y_0^k - Y_0^{k-1})^2} \qquad \text{Eq. A13}$$

that is the patient's motion around kth frame. If there is no motion, V is set equal to zero. Consequently, the contribution from liver (or heart) is thus the total counts inside the ROI. Alternatively, if there is rapid motion, the organ can occupy both regions; thus, V is set equal to one.

Contour Redraw at Each Frame. If large movement occurs during the study, PRDIVA will define the heart and liver contours for each frame. Criterion was used to compare the contour obtained from the beginning of the study with the contour obtained from the end of the study:

$$\Delta = \Delta x/\sqrt{A}, \qquad \text{Eq. A14}$$

where Δx is the distance between the geometric center of the liver contours, and A is the average area within each contour. PRDIVA adjusts the contour threshold L_c of A_1 to make the ratio of these two areas (A_1/A_2) fall between 0.94 and 1.06. If $\Delta > 4\%$, PRDIVA redraws the liver contour at each frame. Blocking out the contribution from the heart by applying a mask, PRDIVA adjusts the contour threshold to make the contours at each frame approximately the same size.

Generation of Time-Activity Curves. In the last step, the liver and heart time-activity curves are generated and written to a file. This file includes every time point, the total counts inside the liver contour W_{liv}^k and the total counts inside heart contour W_{hrt}^k at each time point. Therefore, the counts within the liver contour at the kth frame is:

$$W_{liv}^k = \sum_{i=x_1}^{x_2} \sum_{j=R_{liv}^1(x_i)}^{R_{liv}^2(x_i)} \sigma^k(x_i - X_o^k, y_j - Y_o^k)\,(1 + W_{cb}^k), \qquad \text{Eq. A15a}$$

where $R_{liv}^1(x^i)$, $R_{liv}^2(x^i)$ are the minimum and maximum values in the y-dimension of the liver contour, and x_1 and x_2 are the minimum and maximum values in the x-dimension of the contour. If the contours are repositioned at each frame X_o^k and Y_o^k, as calculated from Equation A3, are applied to correct for the patient's motion and W_{cb}^k, as calculated from Equation A12, is used to correct for blurred images. When the contour redraw algorithm is applied, X_o^k, Y_o^k and W_{cb}^k are set to zero and R_{liv} is defined at each frame as R_{liv}^k. The counts within the heart contour at the kth frame are always calculated using motion and blur correction as:

$$W_{hrt}^k = \sum_{i=x_1}^{x_2} \sum_{j=R_{hrt}^1(x_i)}^{R_{hrt}^2(x_i)} \sigma^k(x_i - X_o^k, y_j - Y_o^k)\,(1 + W_{cb}^k). \qquad \text{Eq. A15b}$$

ACKNOWLEDGMENTS

We thank Dr. Charles E. Metz for his discussions of the ROC analysis, Dusan P. Hutak for excellent technical assistance, Dr. Paul O. Scheibe for helpful suggestions and Dr. Marijana Ivanovic for reviewing the manuscript. This work was supported by U.S. Public Health Service grants RO1 AM34768 and RO1 AM34706.

REFERENCES

1. Stadalnik RC, Kudo M, Eckelman WC, Vera DR. In vivo functional imaging using receptor-binding radiopharmaceuticals: ^{99m}Tc-galactosyl-neoglycoalbumin as a model. *Invest Radiol* 1993;28:64–70.
2. Stockert RJ, Morell AG. Hepatic binding protein. The galactose-specific receptor of mammalian hepatocytes. *Hepatology* 1983;3:750–757.
3. Stadalnik RC, Vera DR, Woodle ES, et al. Technetium-99m-NGA functional hepatic imaging: preliminary clinical experience. *J Nucl Med* 1985;26:1233–1242.
4. Vera DR, Krohn KA, Stadalnik RC, Scheibe PO. [Tc-99m]galactosyl-neoglycoalbumin: in vivo characterization of receptor-mediated binding to hepatocytes. *Radiology* 1984;151:191–196.
5. Vera DR, Krohn KA, Stadalnik RC, Scheibe PO. Technetium-99m-galactosyl-neoglycoalbumin: in vitro characterization of receptor-mediated binding. *J Nucl Med* 1984;25:779–787.
6. Vera DR, Krohn KA, Scheibe PO, Stadalnik RC. Identifiability analysis of an in vivo receptor-binding radiopharmacokinetic system. *IEEE Trans Biomed Engr* 1985;BME-32:312–322.
7. Kudo M, Vera DR, Trudeau WL, Stadalnik RC. Validation of in vivo receptor measurements via in vitro radioassay: ^{99m}Tc-galactosyl-neoglycoalbumin as a prototype model. *J Nucl Med* 1991;32:1177–1182.
8. Kudo M, Vera DR, Trudeau WL, Stadalnik RC. Hepatic uptake of [^{99m}Tc]galactosyl-neoglycoalbumin is sensitive to receptor quantity. *Nucl Med Biol* 1991;18:663–666.
9. Vera DR, Stadalnik RC, Trudeau WL, Scheibe PO. Measurement of receptor concentration and forward binding rate constant via radiopharmacokinetic model of [^{99m}Tc]galactosyl-neoglycoalbumin. *J Nucl Med* 1991;31:1169–1176.
10. Virgolini I, Müller C, Klepetko W, et al. Decreased hepatic function in patients with hepatoma or liver metastasis monitored by a hepatocyte-specific galactosylated radioligand. *Brit J Cancer* 1990;61:937–941.
11. Virgolini I, Müller C, Höbart J, et al. Liver function in acute viral hepatitis as determined by a hepatocyte-specific ligand: ^{99m}Tc-galactosyl-neoglycoalbumin. *Hepatology* 1992;15:593–598.
12. Kudo M, Todo A, Ikekubo K, Yamamoto K, Vera DR, Stadalnik RC. Quantitative assessment of hepatocellular function via in vivo radioreceptor imaging: ^{99m}Tc-galactosyl human serum albumin (Tc-GSA). *Hepatology* 1993;17:814–819.
13. Virgolini I, Kornek G, Höbart J, et al. Scintigraphic evaluation of functional hepatic mass in patients with advanced breast cancer. *Br J Cancer* 1993;68:549–554.
14. Pimstone NR, Stadalnik RC, Vera DR, Hutak DP, Trudeau WL. Evaluation of hepatocellular function via receptor-mediated uptake of a ^{99m}Tc-labeled asialoglycoprotein analogue. *Hepatology* 1994;20:917–923.
15. Vera DR, Scheibe PO, Krohn KA, Trudeau WL, Stadalnik RC. Goodness-of-fit and local identifiability of a receptor-binding radiopharmacokinetic system. *IEEE Trans Biomed Engr* 1992;39:356–367.
16. Metz CE. ROC methodology in radiologic imaging. *Invest Radiol* 1986;21:720–733.
17. Metz CE, Wang P-L, Kronman HB. A new approach for testing the significance of differences between ROC curves measured from correlated data. In: Deconinck F, ed. Information processing in medical imaging. The Hague: Nijhoff, 1984:432–445.
18. Metz CE, Shen J-H, Herman BA. New methods for estimating a binormal ROC curve from continuously distributed test results. 1990 Joint Statistical Meetings of the American Statistical Society and the Biometric Society. Anaheim, CA: American Statistical Society and the Biometric Society; 1990.
19. Vera DR, Stadalnik RC, Metz CE, Pimstone NP. Diagnostic performance of a receptor-binding radiopharmacokinetic model. *J Nucl Med* 1996;37:160–164.
20. Metz CE. Quantification of failure to demonstrate statistical significance: the usefulness of confidence intervals. *Invest Radiol* 1993;28:59–63.
21. Scott AM, Macapinlac H, Zhang J, et al. Image registration of SPECT and CT images using an external fiduciary band and three-dimensional surface fitting in metastatic thyroid cancer. *J Nucl Med* 1995;36:100–103.
22. Pelizzari CA, Chen GTY, Spelbring DR, Weichselbaum RR, Chen C-T. Accurate three-dimensional registration of CT, PET and/or MR images of the brain. *J Comp Asst Tomogr* 1989;13:20–26.
23. Turkington TG, Hoffman JM, Jaszczak RJ, et al. Accuracy of surface fit registration for PET and MR brain images using full and incomplete brain surfaces. *J Comp Asst Tomogr* 1995;19:117–124.
24. Bevington PR. Data reduction and error analysis for the physical sciences. New York: McGraw-Hall, 1969.